Colloid Polym Sci (2006) 284: 700–709
DOI 10.1007/s00396-005-1435-x

ORIGINAL CONTRIBUTION

Mohammed A. Sharaf
Andrzej Kloczkowski
Taner Z. Sen
Karl I. Jacob
James E. Mark

Molecular modeling of matrix chain deformation in nanofiber filled composites

Received: 11 October 2005
Accepted: 23 November 2005
Published online: 14 March 2006

M. A. Sharaf
Department of Chemistry,
Helwan University,
Ain Helwan, Cairo 11791, Egypt

M. A. Sharaf · K. I. Jacob
School of Polymer,
Textile and Fiber Engineering,
Georgia Institute of Technology,
Atlanta, GA 30332-0295, USA

K. I. Jacob
G. W. Woodruff School
of Mechanical Engineering,
Georgia Institute of Technology,
Atlanta, GA 30332-0295, USA

A. Kloczkowski (✉) · T. Z. Sen
L.H. Baker Center for Bioinformatics
and Biological Statistics,
123 Office and Laboratory Bldg.,
Iowa State University,
Ames, IA 50011-0302, USA
e-mail: kloczkow@iastate.edu
Tel.: +1-515-2947261
Fax: +1-515-2943841

T. Z. Sen
Department of Biochemistry,
Biophysics, and Molecular Biology,
Iowa State University,
Ames, IA 50011, USA

J. E. Mark
Department of Chemistry
and the Polymer Research Center,
The University of Cincinnati,
Cincinnati, OH 45221-0172, USA

Abstract The effects of the oriented fiber filler particles on the microscopic properties of the matrix network chains were investigated by using nanofiber filler particles as reinforcing material. Monte Carlo Rotational Isomeric State simulations were carried out for filled poly(ethylene) (PE) networks to study the dependence of the conformational distribution functions of polymer chains and their elastomeric properties on filler loadings. We were especially interested how the excluded volume effect of the nanofiber particles and their orientation (specifically orientational anisotropy) in the matrix influence elastomeric properties of the network. Distribution functions of the end-to-end distances of polymer chains for both unfilled and filled networks were calculated. Effects of nanofiber reinforcements with varying fiber radii and fiber volume fractions were investigated. We have found that the presence of nanofibers significantly increase the non-Gaussian behavior of polymer chains in the composite. The anisotropic effects of the nanofibers on mechanical properties of polymeric composites were studied as a function of their relative orientation to the direction of deformation. The modulus (reduced nominal stress per unit strain) was calculated from the distribution of end-to-end distances of polymer chains using the Mark–Curro method. Relatively small amount of nanofibers was found to increase the normalized moduli of the composite. Our results are quite in satisfactory qualitative agreement with experimental data reported in the literature. This shows that computer simulations provide a powerful tool in predicting physical properties of composite materials.

Keywords Rotational Isomeric State · Monte Carlo · Nanofibers · Fiber reinforcement · Radial distribution function · Poly(ethylene)

Introduction

Composite materials may be defined as materials made up of two or more components forming two or more phases [1]. Such materials must be heterogeneous at least on a microscopic scale. Composite materials may be divided into three general classes according to phase continuity. The first class is particulate-filled materials consisting of a

continuous matrix phase and a discontinuous filler phase made up of discrete particles and the second is the fiber-filled composites. The last class includes skeletal or interpenetrating network composites consisting of two continuous phases. Examples of this class include filled open cell foams and sintered mats or meshes.

Many commercial polymeric materials are composites filled with a wide range of additives. Examples are polyblends and acrylonitrile butadiene styrene materials, foams, filled polyvinyl chloride formulations used in such applications as floor tile and wire coatings, filled rubbers, thermosetting resins containing a great variety of fillers, and glass fiber-filled plastics. There are many reasons for using composite materials rather than the simpler homogeneous polymers. Some of these reasons are increased stiffness, strength, dimensional stability, and impact strength. Also, they show increased mechanical damping, reduced permeability to gases and liquids, modified electrical properties, and reduced cost.

On the other hand, not all of these desirable features are found from any single additive. The advantages that additive materials have to offer must be balanced against their undesirable properties, which include complex rheological behavior, difficult fabrication techniques, and a weakening of some physical and mechanical properties.

The properties of composite materials are determined by the properties of their components, the shape of the filler phase, morphology of the system, and the nature of the interface/interphase. Thus, a great variety of new properties can be obtained with composites just by alteration of their morphological or interface properties. An important property of the interface that can substantially influence mechanical behavior is the strength of the adhesive bond between the phases.

A number of continuum theories that capture the behavior of reinforced composite system can be found in the literature (for a review, see [2]). Because the objective of this work is to characterize composite properties from the molecular aspects of the components, we focus here on determining composite properties from the nature and configuration of the constituent molecules.

Molecular models for reinforcement of polymers

Several theoretical studies were reported on the filler reinforcement phenomena in polymer composites. Ahmed and Jones [3] have provided a review of some of these theories. A good review of much of the earlier work was written by Blanchard and Parkinson [4]. The problem is difficult because of the number of variables involved: the particle size and its distribution, shape, the condition of the surface, and the degree and type of cure are few examples of these variables [5, 6].

Kloczkowski et al. [7] have proposed a new molecular theory to account for the rubber elasticity of filled polymer networks. In this work, it was assumed that the filled polymer network could be represented as a cross-linked mixture of two types of chains attached at one end to spherical filler particles and chains that do not have such attachments. The elastic modulus of the filled polymer was calculated as the sum of contributions from these two types of chains. The elastic moduli of both types of chains were derived from the corresponding distribution functions for their end-to-end distances using Monte Carlo Rotational Isomeric State (MCRIS) technique [7–10]. Chain conformations overlapping filler particles were rejected in the Monte Carlo chain generation process. The calculations were performed for poly(ethylene) (PE) and poly(dimethylsiloxane) (PDMS) chains with various degrees of polymerization. The reinforcement, which is defined as a measure of the difference between the moduli of the attached and free chains, was found to increase with an increase in elongation.

A great deal of experimental data on polymer composites is available, mainly on the reinforcement of natural rubber by carbon black [11–16] and reinforcement of PDMS with precipitated silica or metallic particles [5]. Filler reinforcement was also studied computationally [17–24]. Our previous simulations [2, 7–9, 25] gave pretty good qualitative agreement with these experiments and explained, at least partially, the nature of the filler reinforcement phenomena.

The present theoretical approach

Our approach follows our earlier methodology [26, 27] and is based on the fact that the presence of the filler particles inside the elastomeric matrix changes the distributions for the end-to-end vectors of the nearby chains. This change is due to both the volume excluded to the chains by the filler and the adsorption of the chains onto the filler surface, ultimately influencing the elastic behavior of the polymer network.

In our previous studies [28, 29], ellipsoidal filler particles were inserted into the undeformed polymer network. The present study models the problem of drawing filler fiber particles in the polymer network starting from melted spherical droplets. When the fiber particles become ellipsoids and the system is cooled down for the subsequent stress–strain experiments, polymer chains are already prestretched.

For simplicity, in the present treatment we postpone accounting for the effect of adsorption and focus only on the effect of the excluded volume of the filler particles on the elastomeric behavior of the filled rubber. In addition, we assume that the volume fraction of filler is small so each chain in the polymer network is either unconnected to any filler particle but cross-linked to the polymer network (“free chains”) or attached at only one end to a filler particle (“attached chains”).

The distribution function for a "free" polymer chain located in the vicinity of the filler particle might be partially affected by the presence of filler, but to simplify the model, we have also neglected this effect. Similarly, the probability of a given chain attached at both ends to two different filler particles is small and may be neglected. We assume further that the modulus of the filled elastomer may be expressed as a linear combination of the moduli [f^*] of free chains and attached chains. Specifically,

$$[f^*] = x_{free}[f^*]_{free} + x_{attached}[f^*]_{attached} \quad (1)$$

where x_{free} and x_{attached} are the fractions of the two types of the chains with the latter being proportional to the volume fraction ν_{f} of the filler:

$$X_{attached} = \gamma \nu_f \quad (2)$$

with γ being a proportionality constant. We assume, following Bueche [5] that γ is proportional to the surface area per unit volume of filler, which means that at constant volume fraction of filler within the network, x_{attached} is proportional to the reciprocal diameter of the particles. The parameter γ can be estimated from the experimental data as proposed by Bueche [5].

Generally, the surface of an ellipsoid $\frac{x^2}{a^2}+\frac{y^2}{b^2}+\frac{z^2}{c^2}=1$ is given by a highly complicated formula involving incomplete elliptic integral of the second kind and Jacobi elliptic functions. Fortunately, for the prolate ellipsoids of revolution (a=b) studied by us in this paper, the surface area is given by a relatively simple equation: $S = 2\pi a^2\left[1+\frac{\delta^2}{(\delta^2-1)^{-1/2}}\arccos(1/\delta)\right]$ where $\delta = c/a$ is the aspect ratio. For aspect ratios close to1($\delta \approx 1$), we have $S \approx 2\pi a^2$ and the constant volume of the ellipsoid the surface area is inversely proportional to the major semiaxis c. In addition, because $a^2c = \frac{c^3}{\delta^2} = r^3$ where r is the radius of the fiber droplet, we have $c = r\delta^{2/3}$. This means that surface area is inversely proportional to the radius of the fiber droplet, multiplied by the factor $\delta^{2/3}$. However, for large aspect ratios δ>>1, typical for fiber drawing, the above formula goes to a different limit S=$\pi^2 a^2 \delta^3$. This leads again to the inverse dependence on the radius of the fiber droplet but multiplied, instead of $\delta^{2/3}$, by the factor $\delta^{-7/3}$. For the fixed aspect ratio, the relationship between the surface area of an ellipsoid and the radius of the sphere of the same volume is similar as for spherical particles.

To calculate and compare distribution functions and elastomeric properties of free chains and attached chains, we performed MCRIS simulations for a single polymer chain [30]. The simulations were performed for PE chains (-CH2-)$_{\text{n}}$ with degrees of polymerization n=300 at the temperature 425 K. One should mention that the glass transition temperature T_{g} and the melting temperature T_{m} for low-density PE are in the vicinity of 253 and 388 K, respectively [8, 31].

The three-state isomeric state model is based on the statistical weight matrix [30]

$$\boldsymbol{U} = [u_{\zeta\eta}] = \begin{bmatrix} 1 & \sigma & \sigma \\ 1 & \sigma\psi & \sigma\omega \\ 1 & \sigma\omega & \sigma\psi \end{bmatrix} \quad (3)$$

with

$$u_{\zeta\eta} = \exp\left(-E_{\zeta\eta}/RT\right) \quad (4)$$

where $E_{\zeta\eta}$ is the energy of a pair of skeletal bonds with the $(i-1)^{\text{th}}$ bond being in the state ζ and i^{th} bond in the state η (ζ, η=*trans*, *gauche*$^+$, or *gauche*$^-$). The a priori probability matrix $\boldsymbol{P} = [p_{\zeta\eta}]$ gives the probability of two consecutive bonds (i–1) and i being in conformations ζ and η, respectively. The conditional probability matrix $\boldsymbol{Q} = [q_{\zeta\eta}]$ gives the probability of bond i being in state η, given that bond (i–1) is in state ζ. For chains with large numbers of bonds n, the matrices $\boldsymbol{P}$ and $\boldsymbol{Q}$ become independent of the index i. There are then analytical solutions for $\boldsymbol{P}$ and $\boldsymbol{Q}$ in terms of the eigenvalues λ_1, λ_2, λ_3 of the statistical weights matrix $\boldsymbol{U}$ with λ_1 denoting the largest eigenvalue

$$\lambda_{1,2} = \frac{1}{2}\left[1+\sigma(\psi+\omega) \pm \sqrt{[1-\sigma+(\psi+\omega)]^2+8\sigma}\right] \quad (5)$$

$$\lambda_3 = \sigma(\psi+\omega)$$

The matrix $\boldsymbol{P}$ has the form

$$\boldsymbol{P} = \begin{bmatrix} \frac{1-\lambda_2}{\lambda_1(\lambda_1-\lambda_2)} & \frac{\sigma}{\lambda_1(\lambda_1-\lambda_2)} & \frac{\sigma}{\lambda_1(\lambda_1-\lambda_2)} \\ \frac{\sigma}{\lambda_1(\lambda_1-\lambda_2)} & \frac{\sigma\psi(\lambda_1-1)}{2\lambda_2(\lambda_1-\lambda_2)} & \frac{\sigma\omega(\lambda_1-1)}{2\lambda_1(\lambda_1-\lambda_2)} \\ \frac{\sigma}{\lambda_1(\lambda_1-\lambda_2)} & \frac{\sigma\omega(\lambda_1-1)}{2\lambda_1(\lambda_1-\lambda_2)} & \frac{\sigma\psi(\lambda_1-1)}{2\lambda_2(\lambda_1-\lambda_2)} \end{bmatrix} \quad (6)$$

The conditional probability matrix $\boldsymbol{Q}$ is

$$\boldsymbol{Q} = \begin{bmatrix} \frac{1}{\lambda_1} & \frac{\sigma}{\lambda_1(1-\lambda_2)} & \frac{\sigma}{\lambda_1(1-\lambda_2)} \\ \frac{(1-\lambda_2)}{\lambda_1} & \frac{\sigma\psi}{\lambda_1} & \frac{\sigma\omega}{\lambda_1} \\ \frac{(1-\lambda_2)}{\lambda_1} & \frac{\sigma\omega}{\lambda_1} & \frac{\sigma\psi}{\lambda_1} \end{bmatrix} \tag{7}$$

The elements of matrices $\boldsymbol{P}$ and $\boldsymbol{Q}$ satisfy the normalization conditions

$$\sum_{\zeta,\eta} p_{\zeta,\eta} = 1 \tag{8}$$

$$\sum_{\eta} q_{\zeta\eta} = 1 \tag{9}$$

and

$$\sum_{\eta} p_{\zeta\eta} = \sum_{\eta} p_{\eta\zeta} = p_{\zeta} \tag{10}$$

where p_ζ is the single bond probability for a specified bond being in state ζ.

Our Monte Carlo method of generating representative samples of chain conformations was based on the conditional probability matrix $\boldsymbol{Q}$ shown above. The first skeletal bond of the chain was assumed to be in the *trans* conformation (i.e., ζ was set equal to 1 for the first bond). Random numbers τ from the interval [0.0, 1.0] were generated for the remaining skeletal bonds. For τ in the interval $0 \le \tau < q_{\zeta 1}$, the second bond was assigned a *trans* conformation; for $q_{\zeta 1} \le \tau < \left(q_{\zeta 1} + q_{\zeta 2}\right)$, a *gauche*$^+$ conformation; and for $\left(q_{\zeta 1} + q_{\zeta 2}\right) \le \tau \le 1$, a *gauche*$^-$ conformation. The next bond was assigned the rotational state using the same algorithm but with the row index ζ of the elements $q_{\zeta\eta}$ determined by the conformation of the previous bond (ζ=1, 2, 3 for t, g^+, and g^-, respectively). The process was repeated until the whole chain of n bonds was generated. Large numbers of Monte Carlo chains ($N \ge 20{,}000$) were generated to ensure adequate statistical sampling.

For each chain, the end-to-end vector **r** was calculated from the formula

$$\boldsymbol{r} = (\boldsymbol{E} + \boldsymbol{T}_1 + \boldsymbol{T}_1\boldsymbol{T}_2 + \boldsymbol{T}_1\boldsymbol{T}_2\boldsymbol{T}_3 + \ldots + \boldsymbol{T}_1\boldsymbol{T}_2 \ldots \boldsymbol{T}_{n-1})\boldsymbol{I}_o \tag{11}$$

Here, $\boldsymbol{E}$ is the unit matrix of order 3 and $\mathbf{I}_o$ is the bond vector column (l_o, 0, 0) where l_o is the equilibrium bond length (l_o=1.54 Å). The transformation matrices $\boldsymbol{T}_i$ ($1 \le i \le n-1$) were given by [30]

$$\boldsymbol{T}_i = \begin{bmatrix} \cos\theta_i & \sin\theta_i & 0 \\ \sin\theta_i\cos\phi_i & -\cos\theta_i\cos\phi_i & \sin\phi_i \\ \sin\theta_i\sin\phi_i & -\cos\theta_i\sin\phi_i & -\cos\phi_i \end{bmatrix} \tag{12}$$

The complementary bond angles θ_i are 68.0° for PE and the rotational angles ϕ_i were assumed values 0, 120°, and −120° for conformations t, g^+, and g^-, respectively. The statistical weight parameters used in the calculations were $E_\sigma = 850$ cal/mol, $E_\omega = 1100$ cal/mol, ψ=1, and ω=0 [7, 28, 30]. All the stresses were calculated for deformation ratios α in the range $1.0 < \alpha < 5.0$.

Conformations for a chain in a filler matrix for which any part of the chain overlapped with any one of the nonspherical (fiber) filler particles were rejected. The simulations were continued until $N \ge 20{,}000$ acceptable Monte Carlo chains were accumulated. The resulting values of end-to-end distances r were placed into a histogram to produce the desired end-to-end distance probability distribution function $P(r/r_{\max})$ with $r_{\max} = nl_o$.

We constructed a histogram with 20 equally spaced intervals over the allowed range of distances $0 \le r/r_{\max} \le 1$ because previous studies showed this choice to be the most suitable for obtaining probability distribution functions. This distribution function was obtained by accumulating the numbers of Monte Carlo chains with end-to-end distances within various space intervals and dividing these numbers by the total number N of Monte Carlo chains. The function $P(r/r_{\max})$ was smoothed using the International Mathematical and Statistical Library (IMSL) cubic spline subroutine "cubic spline integration." The smoothing procedure was necessary for the proper calculation of the stress–strain isotherms from the Monte Carlo histogram.

These results can be used directly in the Mark–Curro [26, 27] theoretical method to calculate the elastic properties of any chain from the distribution functions of their end-to-end distances $P(r)$. The distribution $P(r)$ is directly related to the Helmholtz free energy $A(r)$ of a chain having the end-to-end distance r by

$$A(r) = c - k_B T \ln P(r) \tag{13}$$

where c is a constant, T is the temperature and k_B is the Boltzmann constant. Assuming affine deformation, the three-chain model leads to the following general expression for the elastic free energy of the deformed network [26, 27]

$$\Delta A = (\nu/3)\left[A(r_o\alpha_x) + A\left(r_o\alpha_y\right) + A(r_o\alpha_z) - 3A(r_o)\right] \tag{14}$$

Here, ν is the number of moles of chains in the network, α_t (t=x, y, and z) is the deformation ratio in t-direction, and $r_o = < r^2 >_o^{1/2}$ is the value of the root-mean-square of the end-to-end distance of the chains.

The nominal stress f^* (defined as the elastic force at equilibrium per unit cross-sectional area of the sample in the undeformed state) is [32]

$$f^* = -T\left(\frac{\partial \Delta A}{\partial \alpha}\right)_T \tag{15}$$

For uniaxial stretching, substitution of Eq. 14 into Eq. 15 then gives

$$f^* = -(\nu kTr_o/3)\left[G'\left(r_o^{1/2}\alpha\right) - \alpha^{-3/2}G'\left(r_o\alpha^{-1/2}\right)\right] \tag{16}$$

Here $G(r)$=ln $P(r)$ and $G'(r)$ denotes the derivative dG/dr. The IMSL subroutine "derivative of a cubic spline" was used in the numerical calculations of the derivative of the smoothed function $P'(r/r_{\max})$, together with the relation G'=P'/P. The modulus or reduced stress defined as

$$[f^*] = \frac{f^*}{\alpha - \alpha^{-2}} \tag{17}$$

is often fitted to the Mooney–Rivlin semiempirical formula [30]

$$[f^*] = 2C_1 + 2C_2\alpha^{-1} \tag{18}$$

where $2C_1$ and $2C_2$ are constants independent of deformation α. Some of the results will be presented in this form.

In the case of filled networks, however, to account for hydrodynamic effects the deformation α relevant to the elastomeric matrix chains should be replaced by an effective mean amplified extension ratio α_{eff}

$$\alpha_{eff} = \alpha X_{eff} \tag{19}$$

where the amplification factor for spherical filler particles is [11, 32]:

$$X_{eff} = 1 + 2.5\upsilon_f + 14.1\upsilon_f^2 \tag{20}$$

For nonspherical rodlike particles, x_{eff} is given by [32]:

$$X_{eff} = 1 + 0.676\delta\upsilon_f + 1.26\delta^2\upsilon_f^2 \tag{21}$$

where δ is the aspect ratio, defined as the ratio of the length of filler particles to the width.

Oriented nanofiber fillers

The numerical calculations were performed for cross-linked PE chains with n=300 skeletal bonds. The fiber filler particles were placed inside polymer matrix in a highly regular way, forming cubic lattice. The assumption of the cubic lattice arrangements of filler particles significantly simplifies calculations in our model. In our future work we will study more a complicated case of randomly dispersed fiber filler particles. It is assumed that the fiber filler particles are initially spherical droplets of the same radius r_{fib}. The next step is the process of drawing the fiber at the temperature above the melting point of the fiber. We apply the mechanical deformation to the sample and assume that that both polymer chains and fiber droplets respond affinely to the applied external force. If α_x, α_y, and α_z are principal components of the deformation tensor then spherical fiber droplets become ellipsoids with principal semiaxis $\alpha_x r_{\text{fib}}$, $\alpha_y r_{\text{fib}}$, and $\alpha_z r_{\text{fib}}$, respectively. The volume of fiber particles does not change during the drawing and therefore

$$\frac{4\pi r_{fib}^3}{3} = \frac{4\pi r_{fib}^3}{3}\alpha_x\alpha_y\alpha_z \tag{22}$$

i.e., $\alpha_x\alpha_y\alpha_z$=1. In the case of uniaxial extension, all nanofibers are drawn in the same direction and this perfect orientational ordering remains after the quenching of the sample. For uniaxial extension in the z-direction we have α_z=α_d and $\alpha_x = \alpha_y = 1/\sqrt{\alpha_d}$ where the subscript d refers to drawing direction. The aspect ratio δ defined as a ratio of the length to the width of such drawn fiber is

$$\delta = \frac{r_{fib}\alpha_z}{r_{fib}\alpha_x} = \alpha_d^{3/2} \tag{23}$$

The aspect ratio of the fiber δ=100 that we used in our computations leads to unusually high extensions required for the fiber drawing, namely, $\alpha_d = \delta^{2/3} \approx 21.5$. The PE chain composed of 300 units is obviously too short to withhold such large elongations. However, elastic properties of the polymer are derived from the distribution function of the end-to-end distance of polymer chains (calculated by the MCRIS model) by using Mark and Curro's approach [27, 33]. Our past computations [2, 25, 34] show that for sufficiently long chains, end-to-end distance distribution functions have very similar shapes and the elastic properties of chains obtained by Mark and Curro method [27, 33] have very weak dependence on the length of the chain. Because of this, much more computationally costly simulations for very long chains would lead to quite similar results.

The last step of the experiment is classical stress–strain measurements at temperatures below the melting point (but

above the glass transition) of the fiber for previously oriented nanofiber filler particles. In this step, we stretch the sample uniaxially with the deformation ratio α_e. We use the subscript e to distinguish it from deformation ratio of drawing the sample in the previous step of the experiment α_d. We consider now two different cases: (1) when deformation α_e. is applied along the draw direction of the fiber filler and (2) when the direction of deformation is perpendicular to the direction of fiber drawing. In the first case, the total elongation α_{tot} becomes the product of elongation ratio of drawing α_d and the subsequent elongation α_e of the drawn sample.

$$\alpha_{tot} = \alpha_d \alpha_e \tag{24}$$

Assuming that both elongations α_d and α_e were applied in the z-direction, the components of the total elongation ratio are:

$$\begin{aligned} \alpha_{tot,z} &= \alpha_d \alpha_e \\ \alpha_{tot,x} &= \frac{1}{\sqrt{\alpha_d \alpha_e}} \\ \alpha_{tot,x} &= \frac{1}{\sqrt{\alpha_d \alpha_e}} \end{aligned} \tag{25}$$

The nominal stress (see Eq. 16) for stretching parallel to the direction of draw becomes

$$f^* = -(\nu k T r_o/3)\left[G'(r_o \alpha_d \alpha_e) - \alpha_e^{-3/2} G'\left(r_o \alpha_d^{-1/2} \alpha_e^{-1/2}\right)\right] \tag{26}$$

For deformation transverse to the direction of draw (z-direction), e.g., along the x-axis, the total deformation ratios in directions x, y, and z are:

$$\begin{aligned} \alpha_{tot,z} &= \frac{\alpha_d}{\sqrt{\alpha_e}} \\ \alpha_{tot,x} &= \frac{\alpha_e}{\sqrt{\alpha_d}} \\ \alpha_{tot,y} &= \frac{1}{\sqrt{\alpha_d \alpha_e}} \end{aligned} \tag{27}$$

This leads to the following expression for the nominal stress for stretching perpendicular to the direction of draw:

$$f^* = -(\nu k T r_o/3)\left[G'\left(r_o \alpha_e \alpha_d^{-1/2}\right) - \alpha_e^{-3/2}\left\{G'\left(r_o \alpha_e^{-1/2} \alpha_d\right) + G'\left(r_o \alpha_e^{-1/2} \alpha_d^{-1/2}\right)\right\}\right] \tag{28}$$

To estimate the elastic properties of polymer chains in the filled networks, MCRIS calculations were performed with initial undeformed radii r_{fib}=10, 20, 50, and 100 Å.

Results and discussions

Effect of size of oriented nanofibers on the end-to-end distance distributions

Radial distribution functions are highly affected by the size of filler particles. The probability distribution functions $P(r)$ for end-to-end distances r/r_{max} are shown in Fig. 1 for four different volume fractions of the filler expressed as the filler percentage (PF) (D is the edge length of a cubic lattice)

$$PF = 100 \upsilon_f = 100.\frac{4\pi r_{fib}^3}{3D^3} \tag{29}$$

The distribution functions for chains in composites with varying sizes of initially undeformed fiber filler particles (r_{fib}) for a given PF and aspect ratio (δ) show obvious shifts to the left toward smaller values of r/r_{max} in comparison with the unfilled networks. This is a clear indication that the chain dimensions in filled networks undergo a decrease of their dimensions. Such behavior becomes more pronounced with a decrease in the filler radius and an increase in the PF as seen in Fig. 1 and is explainable by the availability of free volume accessible to chain conformations in the composite. The magnitude of the observed shift toward higher values of r/r_{max} for composites with larger fiber particles (e.g., r_{fib}=100 Å) is greater than for small particles (r_{fib}=10 Å).

Effect of anisotropy of shape on the initial dimensions of the chains

The effect of the anisotropic shape of filler particles on the distribution function of polymer chains in the composite is illustrated in Fig. 2. The anisotropic changes of chain dimensions in the oriented filler matrix were calculated in the longitudinal and the transverse direction relative to the fiber drawing axis. Values of $\lambda_{it} = L_{it}/L_{ot}$ (t=x, y, and z) serve as a measure of the change of dimensions of filled

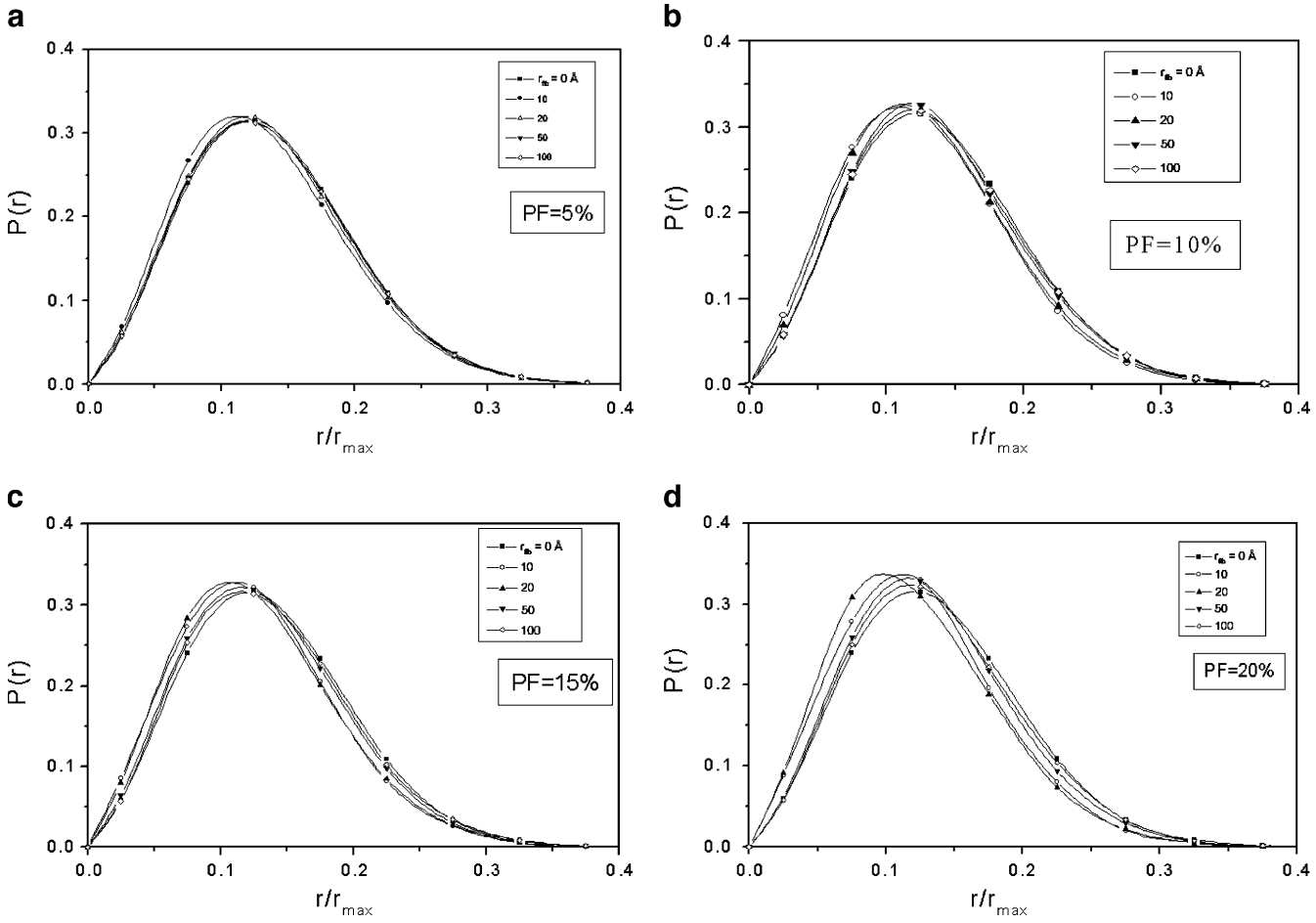

Fig. 1 The radial distribution functions $P(r)$ of the end-to-end distance, obtained by Monte Carlo simulations shown as a function of r/r_{max} at 425 K for PE chains having 300 bonds. The oriented fiber particles having the aspect ratio (δ) of 100, filler percentage (PF) of 5%, and r_{fib} of 10, 20, 50, and 100 Å were arranged on the cubic lattice for PF of (**a**) 5, (**b**) 10, (**c**) 15, and (**d**) 20%

sample relative to the unfilled one before the application of deformation. These values are represented in Fig. 2 as a function of PF at constant aspect ratio (δ) and fiber radius (r_{fib}). Initial chain dimensions in the z-direction are reasonably steady for low fiber volume fractions (0 to 5%), then reduce slightly for intermediate fiber volume fractions (5–12%), and undergo slight increase for higher volume fractions of the filler (Fig. 2a). However, $\lambda_{x,y}$ decreases almost linearly with the increased volume fraction of the fiber (Fig. 2b).

The observed anisotropy in the initial dimensions of polymer chains results from the anisotropy of the oriented fiber filler particles. We should also note that the values of λ_z in Fig. 2a are larger than one (except when PF is equal to 10%), while the values of λ_x (and λ_y) in Fig. 2b are less than one. Such behavior of chain dimensions can be explained by expansion of chains in the direction of the fiber drawing (z) and their shrinkage in perpendicular directions (x and y).

Effect of oriented nanofibers on the reduced modulus

The effect of the oriented fiber particles on the reduced modulus [f^*] as a function of reciprocal effective elongation α_{eff}^{-1} (Eqs. 19, 20, and 21) was also analyzed by applying the Mooney–Rivlin relationship (Eq. 18) [35]. The results of simulations are shown in Fig. 3 with all values of [f^*] normalized by νRT. Figure 3a shows the reduced modulus in the longitudinal z-direction and Fig. 3b in the transverse x-direction relative to the orientation of the drawn fiber.

At small strains (α_{eff}^{-1} close to 1) an increase in the normalized longitudinal modulus is observed (Fig. 3a) as the PFs increases. For intermediate values of α_{eff}^{-1} plot of the reduced modulus is almost linear in agreement with the Mooney–Rivlin formula and values of [f^*] are close to 1—the theoretical value for Gaussian chains. Upturns in the modulus are observed for large elongation (small values of α_{eff}^{-1}), especially when the volume fraction of the oriented

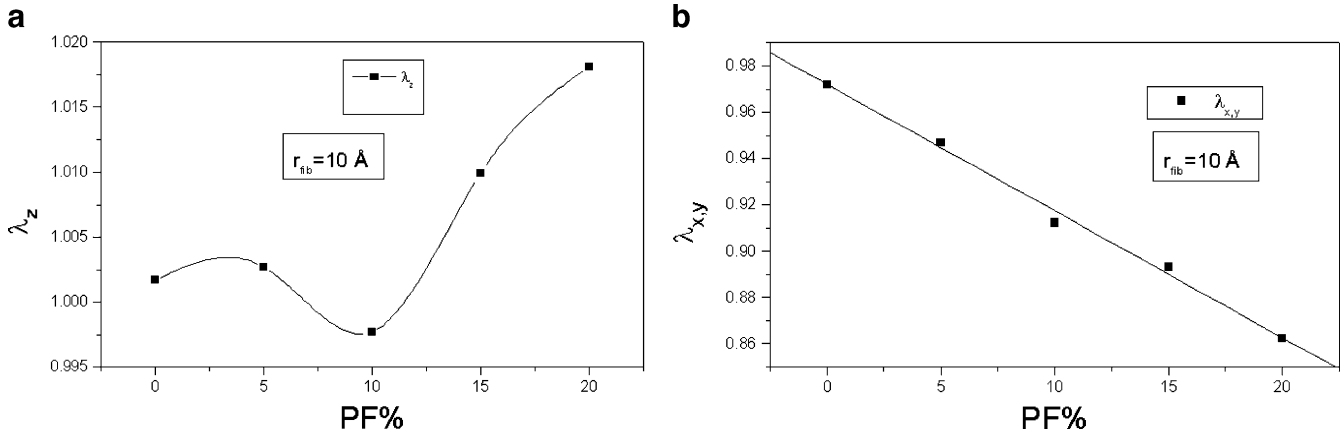

Fig. 2 Anisotropic changes of the initial chain dimensions at 425 K for PE chains having 300 bonds shown as a function of filler percentage (PF) for oriented fiber particles having the aspect ratio (δ) of 100 and r_{fib} of 10 Å along (**a**) the longitudinal direction of the oriented particles (z-axis) and (**b**) the transverse direction of the oriented particles (x-axis)

fiber particles is high (20%). This is obviously the consequence of the finite extensibility of polymer chains that manifests their non-Gaussian behavior. More specifically, these upturns are due to the rapidly diminishing numbers of acceptable configurations at higher values of α, which leads to a significant decrease in the entropy of chains and subsequently the increase of $[f^*]$. Such increases are especially pronounced for fiber particles with higher aspect ratio. Anisotropic increases of the modulus $[f^*]_z$ in the longitudinal direction of fiber drawing (z-axis) comparing to those for unfilled network are clearly apparent, particularly for small elongations. Furthermore, it is clear that a slight change in the size of fiber particles or their volume fraction might have significant effects on values of the modulus. Note that some unusual maxima and minima displayed for high elongations resulted from computational imperfection in the determination of the shape of the distribution function near its maximum. We have observed such oscillatory behavior of the reduced modulus in our previous simulations. It is due to the Mark and Curro [26, 27, 33] method of calculation of the modulus from polymer chain distribution function. It is apparent that for large elongations in the neighborhood of the rapture point, this method shows some limitations.

Figure 3b shows the transverse modulus as a function of the inverse of effective elongation α_{eff}^{-1}. We observe the effects opposite to those seen in Fig. 3a for longitudinal direction. The transverse moduli decrease with the increase of the PF of the oriented fiber particles, especially for small elongations (α_{eff}^{-1} close to 1).

The numerical results presented here are in good qualitative agreement with the experimental data, as comprehensively reviewed by Mark et al. [2]. This is particularly true for the case of rigid particles deformed by compression above their glass transition temperature. One

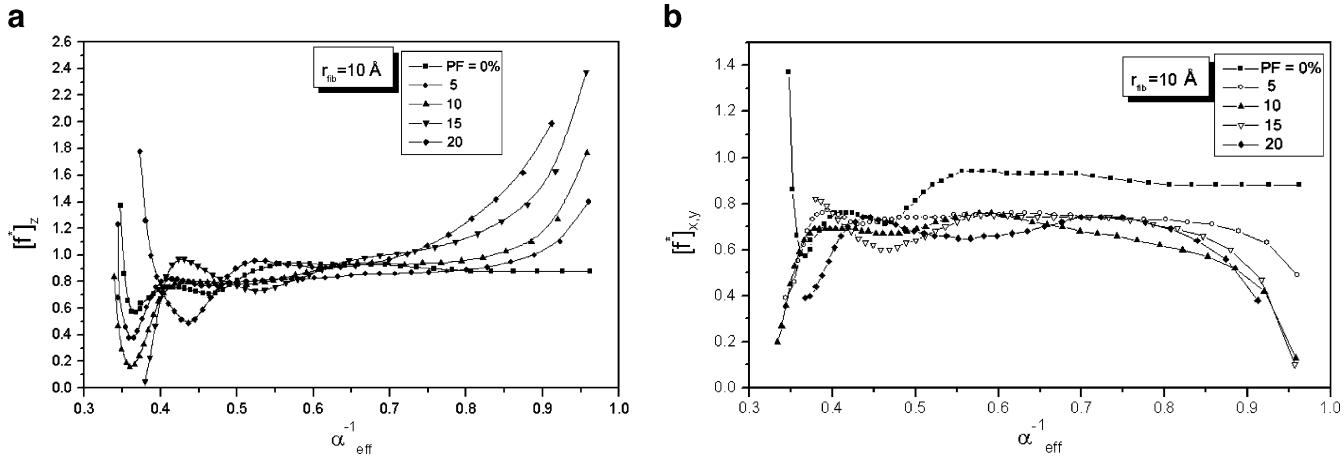

Fig. 3 The (**a**) normalized longitudinal modulus and (**b**) normalized transverse modulus are shown as a function of the inverse effective elongation α_{eff}^{-1} for PE chains having 300 bonds at 425 K for oriented fiber particles having the aspect ratio (δ) of 100, r_{fib} of 10 Å, and filler percentage (PF) of 5, 10, 15, and 20%

should note, however, that our present simulations were restricted to the ideal cubic lattice arrangement of the aligned fiber particles in the composite.

Effect of temperature

The effect of temperature on the distribution function of end-to-end distances of PE chains as a function of r/r_{max} is shown in Fig. 4 for chains attached to filler particles having δ=100, r_{fib}=10 Å, PF=20%, and five different temperatures of 425, 450, 475, 500, and 525 K. At the constant particle size and the volume fraction of the filler, temperature increase shifts distribution toward the left and lowers the value of r_o (position of the peak of the distribution). This can be easily explained by the fact that less extended, energetically costly *gauche* conformations become more populated at higher temperatures leading to a relative shrinkage of chain dimensions.

Statistical weight matrices in the Rotational Isomeric State (RIS) theory depend of the temperature (see Eq. 3). The temperature coefficient of the unperturbed dimensions of the polymer chains can be calculated as ($d \ln\langle r^2\rangle_o/dT$) [6, 28]. This coefficient could be computed directly by using the present numerical method.

Conclusions

In summary, the theoretical method presented here enables the estimation of the effect of the excluded volume of the fiber filler particles having different arrangements in the polymer matrix on the elastomeric properties of the composite. Calculations of reinforcement due to the presence of the filler particles become possible through the use of the RIS method combined with the Mark–Curro [26, 27, 33] simulation approach for non-Gaussian polymeric chains, previously applied to various polymer systems [25, 34]. Induced anisotropy resulted from the fiber drawing during the preparation of the composite is apparent and expressed in distribution functions of polymer chains and their stress–strain isotherms. The reinforcement effect due to the volume exclusion by the filler depends primarily on effective elongation, size and aspect ratio of filler particles, and their volume fraction and, to a less extent, on the detailed chemical structure of polymer chains. In addition, the results are highly sensitive on the relative orientations of the direction of the mechanical deformation during the stress–strain experiment and the direction of fiber drawing applied in the process of the preparation of the composite sample. As discussed in the previous section, oriented fiber filler particles of different radii produce positive reinforcement in the longitudinal direction and negative reinforcement in the transverse direction.

In addition, the theoretical methodology used in the present simulations is relatively simple and should permit for further refinements such as random arrangement of the filler particles and inclusion of physical and chemical adsorption of the polymer chains onto the filler surface. The latter could be done by adding long-range (physical adsorption) and strong short-range (chemical adsorption) interaction potentials between the filler surface and the chain segments.

Finally, we have demonstrated that Monte Carlo simulations could provide significant microscopic insights into the phenomena of reinforcement in polymer-nanofiber composites. To unravel the underlying molecular processes involved in the reinforcement of filled elastomers in a more quantitative way, it is essential to focus on mechanisms of filler–polymer interactions that depend on the detailed structure of their interface and on interactions that lead to agglomeration and aggregation of filler particles. Our

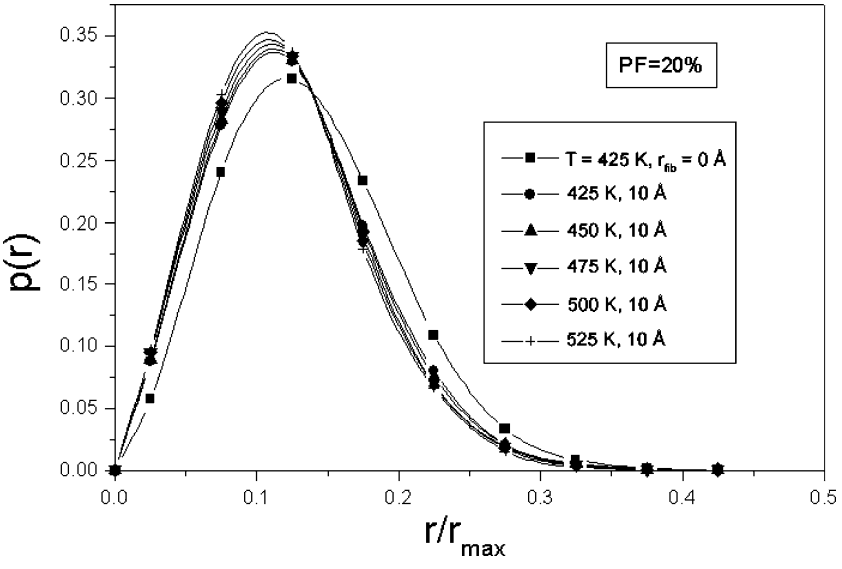

Fig. 4 The radial distribution functions $P(r)$ of the end-to-end distance obtained by Monte Carlo simulations shown as a function of r/r_{max} at temperatures 425, 450, 475, 500, and 525 K for PE chains having 300 bonds. The oriented fiber particles having the aspect ratio (δ) of 100, filler percentage (PF) of 20%, and r_{fib} of 10 Å were arranged on the cubic lattice

simulations indicate that mechanical properties of filled systems depend on the microstructure of the composite and particularly on the shape and orientation of microfibers. More recent neutron scattering results are in excellent agreement with these conjectures, especially regarding the excluded volume effect and the overstrain in filled elastomers [36].

Acknowledgements KIJ and MAS gratefully acknowledge the financial support by The National Textile Center at Georgia Tech. It is also a pleasure to acknowledge the financial support provided by the National Science Foundation through Grants DMR-0314760 (Polymers Program, Division of Materials Research) to JEM and INT-9605191 and INT-0111334 (US-EGYPT International Programs) to JEM and MAS. MAS gratefully acknowledge the financial support provided by US-Egypt Science and Technology Joint Fund through grant MAN7-001-002. AK acknowledges the financial support provided by the NIH grant 1R01GM072014-01. We would like to thank the referee for very helpful comments.

References

1. Lawrence E (1974) Mechanical properties of polymers and composites. Marcel Dekker, New York
2. Mark JE, Abou-Hussein R, Sen TZ, Kloczkowski A (2005) Polymer 46:8894
3. Ahmed S, Jones FR (1990) J Mater Sci 25:4933
4. Blanchard AF, Parkinson D (1952) Ind Eng Chem 44:799
5. Bueche AM (1957) J Polym Sci 25:139
6. Yamakawa H (1971) Modern theory of polymer solutions. Harper & Row, New York
7. Kloczkowski A, Sharaf MA, Mark JE (1993) Comput Polym Sci 3:39
8. Kloczkowski A, Sharaf MA, Mark JE (1994) Chem Eng Sci 49:2889
9. Sharaf MA, Kloczkowski A, Mark JE (1994) Comput Polym Sci 4:29
10. Yuan QW, Kloczkowski A, Mark JE, Sharaf MA (1996) J Polym Sci B Polym Phys 34:1647
11. Guth EJ (1945) Appl Phys 16:20
12. Kraus G (1965) Reinforcement of elastomers. Wiley Interscience, New York
13. Kraus G (1971) Adv Polym Sci 8:155
14. Medalia AI (1970) J Colloid Interface Sci 32:115
15. Medalia AI (1987) Rubber Chem Technol 60:43
16. Porter M (1967) Rubber Chem Technol 40:100
17. Heinrich G, Kluppel M, Vilgis TA (2002) Curr Opin Solid State Mater Sci 6:195
18. Heinrich G, Kluppel M (2002) Adv Polym Sci 160:1
19. Kluppel M (2003) Adv Polym Sci 164:1
20. Lin H, Erguney F, Mattice WL (2005) Polymer 46:6154
21. Ozmusul MS, Picu CR, Sternstein SS, Kumar SK (2005) Macromolecules 38:4495
22. Vacatello M (2003) Macromol Theory Simul 12:86
23. Vacatello M (2004) Macromol Theory Simul 13:30
24. Vacatello M (2001) Macromolecules 34:1946
25. Sen TZ, Sharaf MA, Mark JE, Kloczkowski A (2005) Polymer 46:7301
26. Mark JE, Curro JG (1983) J Chem Phys 79:5705
27. Mark JE, Curro JG (1984) J Chem Phys 80:5262
28. Sharaf MA, Kloczkowski A, Mark JE (2001) Comput Theor Polymer Sci 11:251
29. Sharaf MA, Mark JE (2002) Polymer 43:643
30. Flory P (1969) Statistical mechanics of chain molecules. Wiley Interscience, New York
31. Mark JE, Erman B (1988) Rubberlik elasticity. A molecular Primer. Wiley Interscience, New York
32. Heinrich G, Vilgis TA (1993) Macromolecules 26:1109
33. Curro JG, Mark JE (1984) J Chem Phys 80:4521
34. Kloczkowski A, Sen TZ, Sharaf MA (2005) Polymer 46:4373
35. Lee LH (1969) J Polymer Eng Sci 9:213
36. Wu D, Hui K, Chandler D (1992) J Chem Phys 96:835